Follow us @BoneJointRes

Freely available online OPEN ACCESS

BJR

BIOMECHANICS

The effect of plate design, bridging span, and fracture healing on the performance of high tibial osteotomy plates

AN EXPERIMENTAL AND FINITE ELEMENT STUDY

A. R. MacLeod,
G. Serrancoli,
B. J. Fregly,
A. D. Toms,
H. S. Gill

University of Bath, Bath, United Kingdom

Objectives

Opening wedge high tibial osteotomy (HTO) is an established surgical procedure for the treatment of early-stage knee arthritis. Other than infection, the majority of complications are related to mechanical factors – in particular, stimulation of healing at the osteotomy site. This study used finite element (FE) analysis to investigate the effect of plate design and bridging span on interfragmentary movement (IFM) and the influence of fracture healing on plate stress and potential failure.

Materials and Methods

A 10° opening wedge HTO was created in a composite tibia. Imaging and strain gauge data were used to create and validate FE models. Models of an intact tibia and a tibia implanted with a custom HTO plate using two different bridging spans were validated against experimental data. Physiological muscle forces and different stages of osteotomy gap healing simulating up to six weeks postoperatively were then incorporated. Predictions of plate stress and IFM for the custom plate were compared against predictions for an industry standard plate (TomoFix).

Results

For both plate types, long spans increased IFM but did not substantially alter peak plate stress. The custom plate increased axial and shear IFM values by up to 24% and 47%, respectively, compared with the TomoFix. In all cases, a callus stiffness of 528 MPa was required to reduce plate stress below the fatigue strength of titanium alloy.

Conclusion

We demonstrate that larger bridging spans in opening wedge HTO increase IFM without substantially increasing plate stress. The results indicate, however, that callus healing is required to prevent fatigue failure.

Cite this article: *Bone Joint Res* 2018;7:??–??.

Keywords: Osteotomy, Plate, Stress

■ A. R. MacLeod, MEng, PhD, Research Associate,

■ H. S. Gill, BEng, DPhil, CEng, FIPEM, FHEA, Professor of Mechanical Engineering, Department of Mechanical Engineering, University of Bath, Bath, UK.

■ G. Serrancoli, BEng, PhD, Lecturer, Department of Mechanical Engineering, Polytechnic University of Catalonia, Barcelona, Catalunya, Spain.

■ B. J. Fregly, BEng, PhD, Professor and CPRIT Scholar in Cancer Research, Department of Mechanical Engineering, Rice University, Houston, Texas, USA.

■ A. D. Toms, MBChB, FRCS(Ed), MScEng, FRCS(Tr&Orth), Honorary Clinical Professor, Princess Elizabeth Orthopaedic Centre, Royal Devon and Exeter NHS, Exeter, UK.

Correspondence should be sent to A. R. MacLeod; email: a.macleod@bath.ac.uk

doi: 10.1302/2046-3758.712.BJR-2018-0035.R1

Bone Joint Res 2018;7:1–11.

Article focus

- The influence of working length when using different opening wedge designs of high tibial osteotomy (HTO) plates.
- The influence of healing on HTO plate stress reduction when using different plate designs.

Key messages

- Larger bridging spans in opening wedge HTO increase interfragmentary movement (IFM) without substantially increasing plate stress.
- Osteotomy gap healing is required to prevent plate fatigue failure.

Strengths and limitations

- This is an experimentally validated computational study.
- Several situations were evaluated involving different screw configurations and stages of healing.

Introduction

The lifetime risk of knee osteoarthritis (OA) is estimated to be as high as 45%[1] and is

becoming more common.[2] Although the demand for knee arthroplasty is predicted to double by 2030,[3] it is only suitable for end-stage disease.[4] High tibial osteotomy (HTO) is an established treatment for early-stage knee arthritis. The procedure uses an opening or closing wedge osteotomy to change the varus alignment to a more valgus alignment, thereby altering the mechanical axis of the leg and reducing the load in the painful compartment.[5] The osteotomy is then stabilized using an osteosynthesis plate. Plates with angularly stable 'locking' screws are generally used to ensure the osteotomy angle is maintained, since conventional screws have been shown to subside after the operation.[6,7] Opening wedge HTO procedures are more popular[8] due to the simpler surgical approach, lower risk of peroneal nerve damage,[9,10] and better postoperative flexion scores.[10] Unfortunately, the overall complication rate is still relatively high at 31%.[11] Infection is generally the most common complication (approximately 10%),[11] while reported rates of nonunion and delayed union range from 4.3% to 8.2%,[11-13] and rates of implant breakage range from 4.4% to 10%.[14,15] Patients with delayed consolidation of the osteotomy have been reported to have a significantly ($p < 0.05$) greater likelihood of complications.[14] Therefore, due to the importance of preventing nonunions and delayed unions from occurring, promotion of fracture healing should be a priority in HTO surgery.[16]

In studies by Spahn et al[15] and Nelissen et al,[17] more plate breakages occurred in the non- or restricted-weight-bearing groups than in the fully weight-bearing groups. This observation implies that the loads imposed on the plate are not the only factor influencing plate breakage. While weight-bearing loads cause plate deformation, they also induce interfragmentary movement (IFM), stimulating healing at the fracture site, which in turn reduces stress on the plate.[18] It is well known that wider fracture gaps require larger movements to achieve the same strain environment,[19] and, unsurprisingly, the likelihood of HTO complications is related to the size of the osteotomy angle.[15] Therefore, with the exception of infection, the most common complications in opening wedge HTO are related to mechanical factors and, in particular, the stimulation of healing at the osteotomy site.

Previous biomechanical studies have investigated the static strength and fatigue resistance of HTO plates. TomoFix HTO plates (DePuy Synthes, Zuchwil, Switzerland) have been shown to have lower stiffness and migrate more with cyclical loading than iBalance (Arthrex GmbH, Munich, Germany), Contour Lock (Arthrex), and PEEKPower (Arthrex) implants.[20] Despite these findings, TomoFix implants (without wedge blocks) are still the gold standard in HTO treatment and have lower complication rates than short spacer plates designed by competitors.[21] In laboratory-based studies, implants that produce higher construct stiffness also generally have greater fatigue resistance.[20,22,23] Clinically, however, more flexible implants can perform better in terms of healing,[24] indicating that mechanical properties such as strength and, more importantly, stiffness do not necessarily translate into improved clinical performance.

It is difficult to recreate the *in vivo* biomechanical environment *in vitro*. For example, it is not practical to incorporate muscle forces in laboratory experiments. Additionally, fatigue tests in a laboratory setting ignore the fact that the osteotomy will heal over time, making it difficult to predict medium- or long-term *in vivo* performance.[20] Computer simulation allows the prediction of variables that would be difficult or impossible to measure experimentally. However, the model must be thoroughly validated to ensure it represents reality[25], and minimum reporting guidelines aid reproduction and improve standards.[26] Some previous computational studies have investigated implant stress,[27-29] IFM within the osteotomy,[28,29] and the influence of plate design.[30] A major limitation of previous computational studies using locking plates, however, is the use of bonded plate-screw interfaces. This assumption dramatically increases the construct stiffness while also lowering predictions of plate stress.[31] Additionally, previous HTO computational studies have not considered the influence of healing at the fracture site.

The aim of this study was to create and validate a computational model of a tibia following an HTO procedure in order to compare predictions of IFM, plate stresses, and bone strains for different plate spans and designs. The three main goals of the investigation were: 1) to evaluate the influence of different screw arrangements – in particular, to assess whether a longer bridging span using fewer screws could be used safely; 2) to compare a custom HTO plate against an existing design; and 3) to investigate the influence of callus healing on the predictions of plate stress and bone strain.

Materials and Methods

The study was performed in three stages: 1) experimental testing; 2) creation of a finite element (FE) model validated for the intact condition and for an HTO procedure performed using a custom plate design and two different screw configurations; and 3) investigation of the influence of different plate configurations under physiological loading and including healing fracture callus.

Experimental testing

A composite surrogate tibia was selected for use in the study (third-generation Sawbones model 3302, Biomechanical Test Materials; Pacific Research Laboratories, Malmö, Sweden). The specimen was instrumented with tri-axial strain gauges (SGD-2/350-RY63; Omega Engineering Ltd, Manchester, UK) at five locations of interest (Fig. 1a) based on a preliminary computational

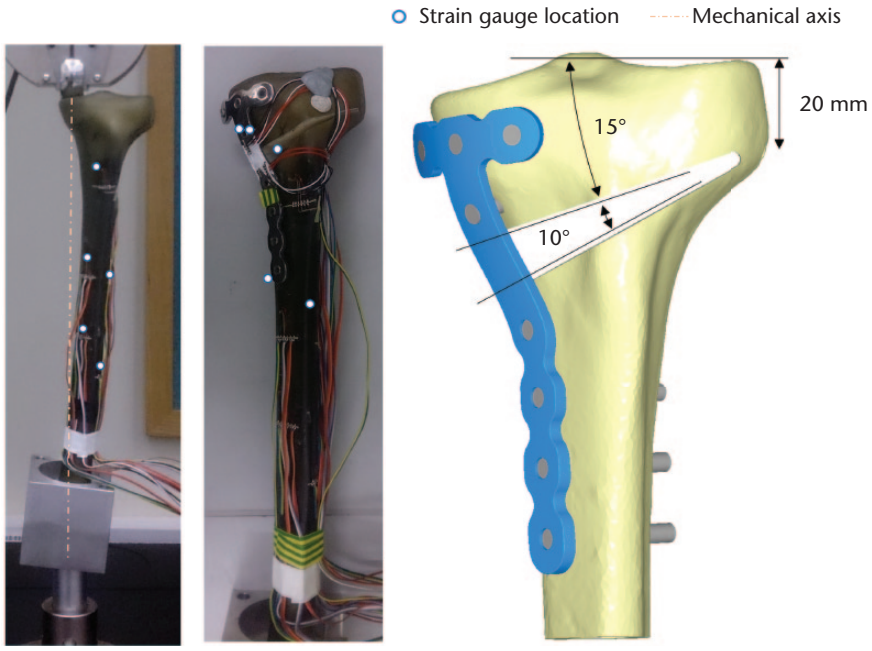

Fig. 1a Fig. 1b Fig. 1c

a) The location of the five strain gauges used on the intact sawbones specimen in the testing machine. b) The osteotomized and plated sawbones specimen. c) The geometry of the osteotomy.

study. The composite tibia was potted using a low melting point alloy (Wood's Metal (70°C); Lowden Metals Ltd, Halesowen, United Kingdom) and mounted in a materials testing machine (Series 5965; Instron, Norwood, Massachusetts). The distal tibia was restrained using a 20 mm diameter spherical bearing positioned at the centre of the ankle joint. A unicondylar knee arthroplasty femoral component (Medium Oxford Partial Knee; Zimmer Biomet, Swindon, United Kingdom) with a radius of 23 mm was used to secure the specimen proximally and apply the loading to the medial condyle (Fig. 1a). The load was applied along the axis from the medial condyle to the ankle (Fig. 1a) in increments of 50 N up to 500 N. Strain readings were recorded using data acquisition software (LabVIEW 2010; National Instruments Corporation (U.K.) Ltd, Newbury, United Kingdom). Maximum and minimum principal strains were calculated from the measured directional surface strains (Matlab R2015b; The Mathworks Inc., Natick, Massachusetts). Each test was repeated ten times and the average was calculated.

After testing in the intact condition, a wedge osteotomy was created (AO classification: 31-A1 / 31-A2). The proximal plane of the resulting osteotomy was inclined 15° to the joint line at the knee, and the gap angle was 10° (Figs 1b and 1c). A custom HTO locking plate was designed to match the surface profile of the composite tibia and manufactured using titanium alloy (Ti-6Al-4V) (EOS M:280 laser sintering; Mario Nava S.p.A., Bosisio Parini, Italy). The profile of the plate used locations on the surface of the specimen obtained from a micro-CT scan of the composite tibia (Nikon XTH225 ST CT-scanning unit; Nikon UK Ltd, Kingston upon Thames, United Kingdom). Locking screws were also manufactured; the threads were tapped/threaded as post-processing operations. The plate was located against the bone using a custom positioning jig to ensure it was placed exactly as planned in the virtual environment. Tri-axial strain gauges were also applied to the top and bottom surfaces of the locking plate (Fig. 1b). The plated, osteotomized tibia was then tested in an identical manner to the intact specimen. In total, three scenarios were examined: A) an intact tibia; B) an osteotomized tibia stabilized with the custom plate using a short bridging span with four distal locking screws; and C) an osteotomized tibia stabilized with the custom plate using a long bridging span with three distal locking screws (Fig. 2). The working lengths for the short and long bridging spans considered in our study were 33 mm and 50 mm, respectively, for both plate types. As we were limited to recording 15 strain readings simultaneously (three per strain gauge), during the testing of conditions B and C, two of the bone strain gauges were unused during testing of the implanted tibia. In order to measure IFM in a non-contact manner, the net displacement of two tracking markers was determined using digital image correlation software (Ncorr v1.2; Georgia Institute of Technology, Atlanta, Georgia). The tracking markers were applied to the surface of the bone above and below the osteotomy, and photographs were taken every 100 N during loading (Matlab R2016b; The

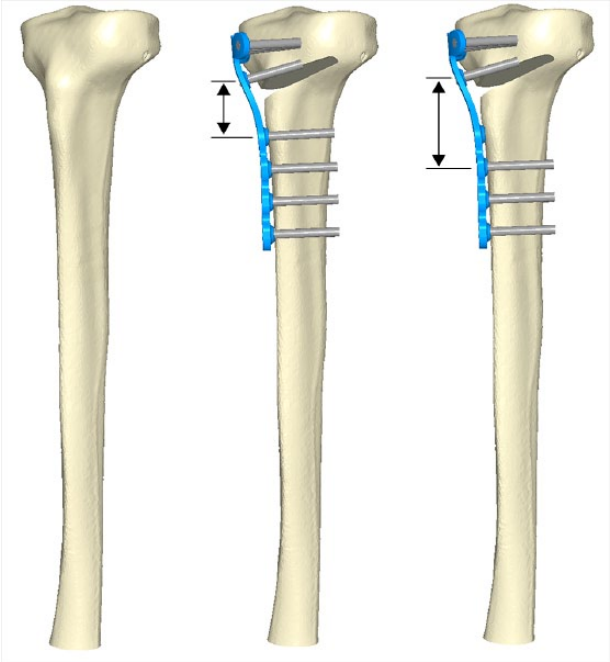

Fig. 2a Fig. 2b Fig. 2c

The different scenarios examined experimentally, showing: a) the intact tibia; b) the first screw configuration with a short bridging span annotated (plate superimposed for clarity); and c) the second screw configuration with a longer bridging span annotated.

MathWorks, Inc.) using a digital camera (DFK 23GP031, Resolution: 2592×1944 (5 MP); Imaging Source Europe GmbH, Bremen, Germany).

Finite element modelling: validation. For validation purposes, FE models were created to replicate the three experimental cases A, B, and C (Abaqus 2017, Simulia; Dassault Systèmes, Paris, France). The Sawbones tibia geometry was created from the previously acquired CT scan using image processing software (ScanIP version M-2017.06; Synopsys, Mountain View, California). Material properties of the surrogate cortical and cancellous bone were assigned based on the manufacturer's information (Pacific Research Laboratories). Linear elastic isotropic material properties were used with Young's moduli (Poisson's ratio) equal to 7.6 GPa (0.24) and 157 MPa (0.3) for cortical and cancellous bone, respectively.

Screws were modelled as cylinders with an outer diameter of 5.0 mm. As the interest of the study was primarily the IFM and plate stress, the screw-bone interaction was modelled as tied for simplification.[32] The screw-plate interface was modelled as a penalty-based interaction with a tabulated contact stiffness (Table I) and a standard Coulomb friction model with coefficient of friction equal to 0.8 to represent the macro-interlock of the plate and screw threads mating. Similar values of friction have been used previously to represent rough screw-bone interfaces.[33]

Reference points representing the experimental proximal and distal centres of rotation (knee and ankle) were defined. These reference points were rigidly connected to the bone surface using a multi-point constraint. The proximal reference point was restrained against transverse movement but allowed to move along the mechanical axis. The distal reference point was restrained against all translations. The load was applied proximally in the same manner as the experimental tests.

Table I. The pressure-over closure relationship of the plate-screw contact

Pressure (MPa)	Overclosure (mm)
0	-0.01
10	0.05
100	0.1
1000	1

The FE models were solved using geometric non-linearity with an implicit solver and automatic incrementation (Abaqus 2017). The models were meshed using fully integrated quadratic tetrahedral elements (C3D10), with an average element edge length of 0.8 mm for the plate, 0.8 mm for the screws, 1.4 mm for the cancellous foam, 1.2 mm for the cortical shell, and 2.0 mm for the callus. In contacting regions, the average element edge length was refined to 0.5 mm. The total number of nodes and elements was 1 050 282 and 769 227, respectively. A mesh convergence study was conducted (convergence criteria, 5%). For the selected mesh resolution, doubling the mesh size altered the prediction of IFM by 3.20%, plate stress by 0.54%, and principal strain in the bone around screw holes by 3.89%.

The predicted principal strains and IFM from the FE models were compared against the experimentally measured values using linear regression.

Finite element modelling: incorporating physiological loading. After validation, a physiological loading case was incorporated. We chose to use the instance of the gait cycle where the medial knee joint contact forces are highest, corresponding to 19% of the gait cycle.[34] Muscle and joint contact forces for a 70 kg patient from a previous study[34] were registered to our geometry (Matlab R2016b). All forces were applied at reference points and distributed over the surface of the bone within a 10 mm to 12 mm radius (Fig. 3). In these models, the most distal part of the tibial shaft was constrained in all directions and no other restraint was applied (Fig. 3). The muscle force and joint reaction vectors are given in Table II.

Finite element modelling: structural optimization of plate. The shape of the custom plate was structurally optimized for the short and long configurations under physiological loading (Tosca Structure 2017, Simulia; Dassault Systèmes). The optimization process iteratively modified the envelope of the geometry in order to satisfy prescribed optimization functions. Our intention was to reduce the maximum plate stress while increasing the average plate strain to generate IFM. Two equally weighted design optimization functions were used: 1)

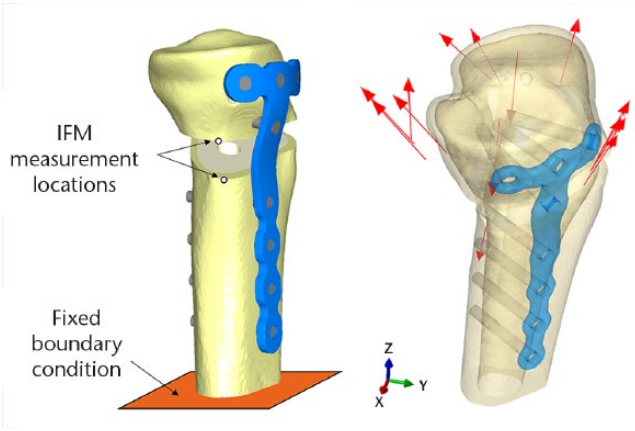

Fig. 3a Fig. 3b

a) The measurement locations used to determine the interfragmentary movement (IFM) experimentally and in the finite element (FE) models; b) the locations of the applied muscle force vectors (not to scale).

Table II. Joint contact and muscle forces applied to the model; the coordinate system is shown in Figure 3b

Force description	Directional force component (n)		
	x	y	z
Medial knee joint contact force	45.35	8.84	-984.14
Lateral knee joint contact force	16.09	3.14	-349.25
Biceps femoris (long head)	1.13	-5.59	4.65
Biceps femoris (short head)	1.41	-3.47	6.00
Gracilis	1.30	-23.30	23.45
Rectus femoris	24.36	21.93	74.34
Sartorius	1.16	-0.01	3.35
Semimembranosus	-0.69	-31.74	29.12
Semitendinosus	0.15	-5.71	5.38
Soleus	-7.15	-3.31	-26.39
Tensor fasciae latae	39.34	24.63	191.36
Vastus intermedius	22.83	27.63	78.72
Vastus lateralis	3.11	4.01	13.25
Vastus medialis	52.57	48.36	141.60

Table III. Callus properties assumed for different stages of bone fracture healing[34,35]

Approximate postoperative time, wks)	Tissue type	Young's modulus (MPa)	Poisson's ratio
0	No callus	N/A	N/A
1	Connective tissue	1.4	0.33
2	Fibrous tissue	28.0	0.3
6	Woven bone	528.0	0.3

the maximum strain energy density (SED) anywhere in the plate; and 2) the negative of the minimum SED in the bridging span of the plate. The maximum values of both functions were minimized until the combined SED function was deemed to have converged; at 20 design cycles there was 0.12% change from the previous iteration. Geometric restrictions were placed on the screw holes, and the volume of the plate was constrained to a fraction of 0.9 of the original plate to help reduce underused material. The resulting shape of the optimized plate mesh was smoothed and re-exported.

Finite element modelling: comparison of different plate types with callus healing. The FE model was modified to replace the custom plate with a widely used commercial HTO device (TomoFix; DePuy Synthes). The geometry of the TomoFix plate was obtained by reconstructing micro-CT scan data in a similar manner to the bone geometry. Other than the plate geometry, all aspects of the TomoFix model were identical to the custom plate model. For both plate types, predictions were made for short and long bridging spans. The fracture callus was represented by filling the osteotomy gap with a linearly elastic isotropic homogeneous material. Three stages of early callus healing were incorporated into the models: connective tissue formation; fibrous tissue formation; and immature woven bone formation. Young's modulus and Poisson's ratios for each stage are given in Table III.[35,36]

Measured output variables. The main variables of interest in the study were the IFM and the peak von Mises stress within the plate. The IFM was defined as the difference in displacement between the measurement locations at the osteotomy site (Fig. 3). Axial IFM was calculated using displacement along the mechanical axis (z-direction), whereas transverse IFM was calculated using the magnitude of the transverse displacements (x- and y-directions). Additionally, the strain levels in the cortical bone around the screw holes were evaluated. A measure of strain concentration, termed εVOL, was used as an output variable, defined as the total volume of bone exposed to a principal strain larger than the cortical bone yield strain of either 0.5% in tension or 0.7% in compression.[37]

Results

Evaluation of finite element model. The principal strain predictions of the FE models closely correlated with the experimentally measured data (Fig. 4). The linear regression slope (and R^2) values for cases A, B, and C were 0.77 (R^2 = 0.96), 1.13 (R^2 = 0.98), and 1.06 (R^2 = 0.98), respectively. The values of measured and predicted axial interfragmentary displacement (IFM) were within 5% at 500 N with a root mean square error (RMSE) of 0.03 mm and 0.02 mm for the short and long bridging spans, respectively (Fig. 5a). Linear regression of the IFM predictions against measured values gave slope (and R^2) values of 0.99 (0.996) and 0.94 (0.995) for cases B and C, respectively (Fig. 5b).

Comparison of TomoFix and optimized custom plate. The shape optimization process resulted in the custom plate becoming thicker and wider over the bridging span and around the two screw holes on either side of the

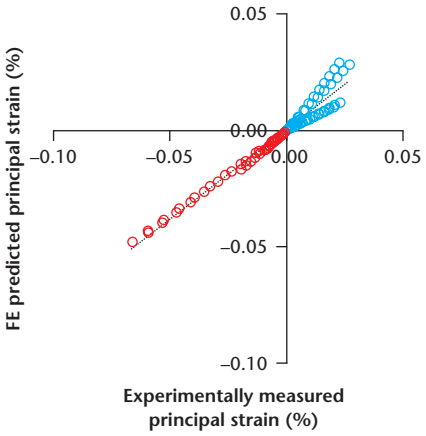

Fig. 4a

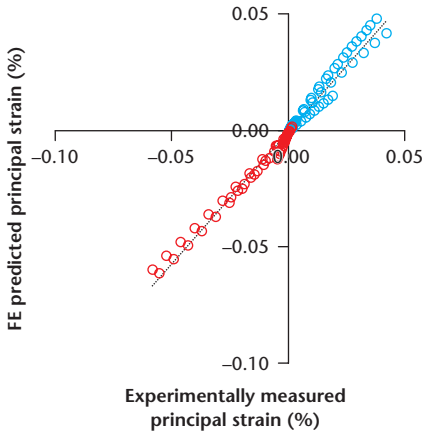

Fig. 4b

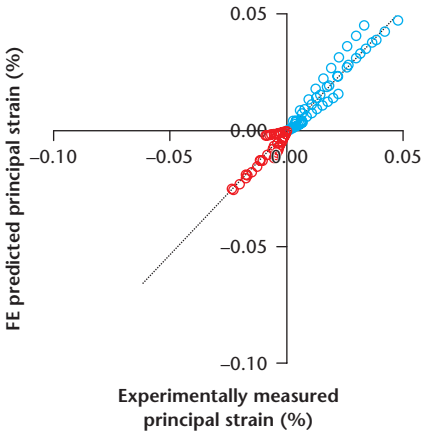

Fig. 4c

Maximum (blue) and minimum (red) principal strain at the five strain gauge locations for: a) the intact tibia; b) the stabilized osteotomized tibia with short span; and c) the stabilized osteotomized tibia with long span.

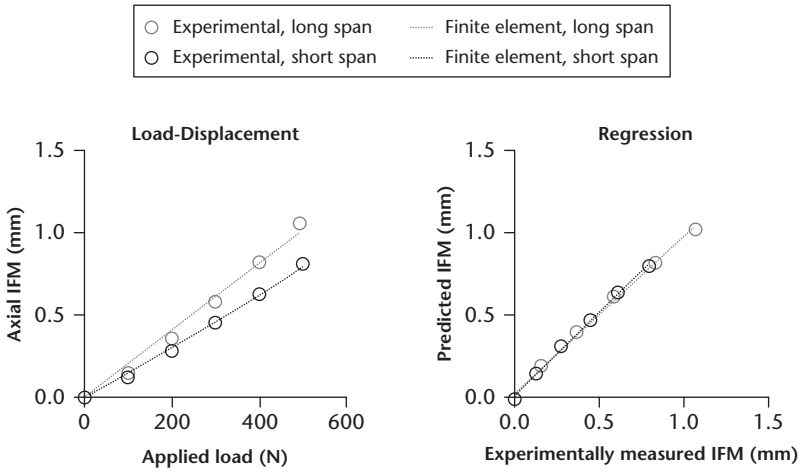

Fig. 5a

Fig. 5b

a) Values of axial interfragmentary movement (IFM) measured experimentally and finite element (FE) predictions for two different screw arrangements. b) Linear regression of the predicted *versus* measured IFM values.

osteotomy. Compared with the pre-optimized design, the average plate stress increased while the maximum stress decreased. The underside of the plate also became concave.

Comparing the optimized custom plate against the TomoFix plate, the pattern of IFM produced by the two devices was similar (Fig. 6). The custom plate produced a 4.8% smaller axial IFM than did the TomoFix device in the short bridging span but a 24.1% larger axial IFM in the long bridging span. In the custom plate, shear IFM was increased by 52.1% and 54.8% for short and long bridging spans, respectively (Fig. 6a). The values of IFM underneath the plate followed the same trends as those at the IFM measurement locations (Fig. 6b).

In both configurations, the TomoFix plate experienced peak plate stresses at the screw hole proximal to the osteotomy and the plate T-junction, whereas the custom plate distributed the stresses more evenly throughout the span bridging the osteotomy (Fig. 7). For the TomoFix, the peak von Mises stress was 656 MPa and 654 MPa for short and long bridging configurations, respectively. For the custom plate, the peak stress was 693 MPa for the short span and 715 MPa for the long span. The peak von Mises stress within the custom plate was 5% larger than with the TomoFix plate for the short span and 10% larger for the long span.

Strains in the bone around screw holes. The distribution of strain in the bone around screw locations was different for the two plate types (Fig. 8). For both bridging spans, the TomoFix plates produced larger εVOL around the metaphyseal screw holes compared with the custom plate (Fig. 9), particularly screw holes 1 and 3. The TomoFix plate also produced larger εVOL at the most distal screw (number 8). Compared with the TomoFix, the custom plate produced slightly larger εVOL around the screws adjacent to the osteotomy (numbers 4 and 5) compared with the TomoFix plate. Compared with

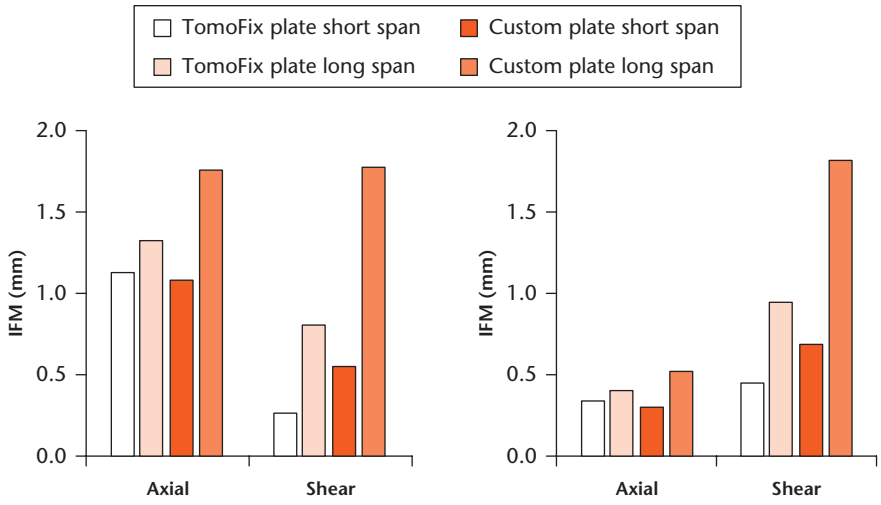

Fig. 6a

Fig. 6b

Net axial and transverse interfragmentary movement (IFM) for both plate types and spans under physiological loading with joint contact and muscle forces corresponding to 19% of the gait cycle, showing a) the IFM at the medial measurement locations (Fig. 3) and b) the IFM under the plate.

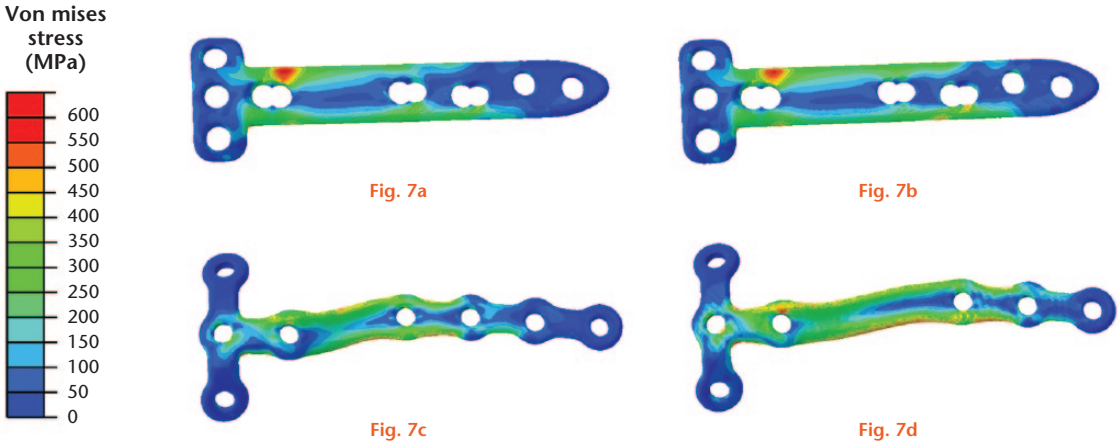

Fig. 7a

Fig. 7b

Fig. 7c

Fig. 7d

Predicted von Mises stress within the plate assuming no callus formation for: a) the TomoFix plate with a short bridging span; b) the TomoFix plate with a long bridging span; c) the custom plate with a short bridging span; and d) the custom plate with a long bridging span. Red regions have values higher than 600 MPa.

the short span, the longer span produced 44.1% and 61.1% larger εVOL for the custom plate and the TomoFix, respectively. The εVOL for the custom plate was 32.5% smaller and 39.6% smaller than that of the TomoFix for the short and long spans, respectively. Considering only the screws in metaphyseal bone, the custom plate reduced εVOL by 61.2% and by 51.9% for the short and long spans, respectively.

Influence of fracture callus. As the stiffness of the callus increased, the stress in both plate types decreased (Fig. 10). Peak von Mises stress in the TomoFix plate was very similar for both span lengths. The custom short span plate produced lower peak stress compared with the custom long span plate. The peak stress was higher than the fatigue strength of titanium for all cases, except when a callus stiffness of 528 MPa was used (corresponding to immature woven bone).

Discussion

This study investigated the biomechanical environment produced by two HTO plate types under physiological loading. Different bridging spans were considered by changing the number of screws used. The study was performed using a validated FE model and demonstrated that longer bridging spans did not necessarily increase plate stress. When early callus formation was included in the models, the plate stress was similar or lower for the longer bridging spans compared with the shorter bridging spans.

By using an optimization algorithm to increase the average plate strain while minimizing the maximum plate strain, we produced a custom plate that produced higher IFM and smaller regions of high strain in the bone compared with the TomoFix design with similar levels of peak stress. It should be noted that if plate stress was the only

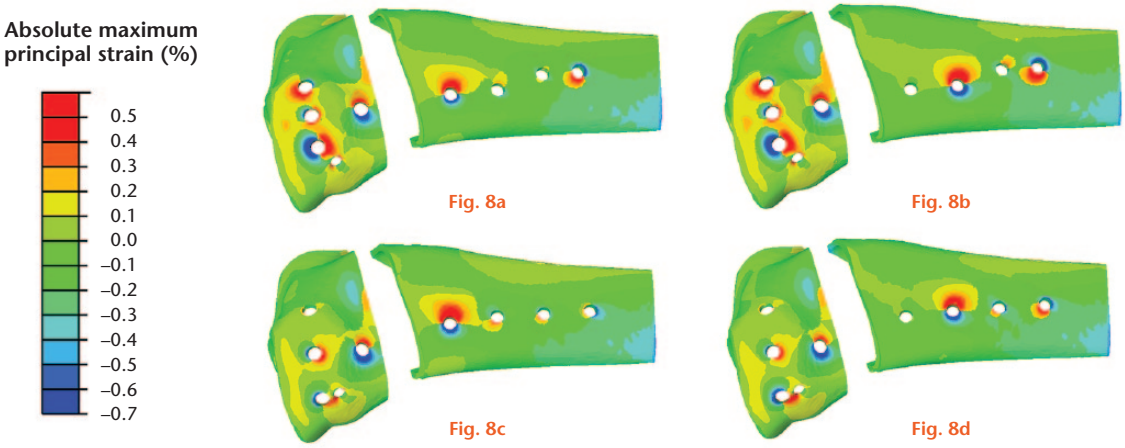

Predicted absolute maximum principal strain on the surface of the tibia for: a) the TomoFix plate with a short bridging span; b) the TomoFix plate with a long bridging span; c) the custom plate with a short bridging span; and d) the custom plate with a long bridging span. Red and blue regions have values higher than 0.5% (tensile) and -0.7% (compressive) strain, respectively.

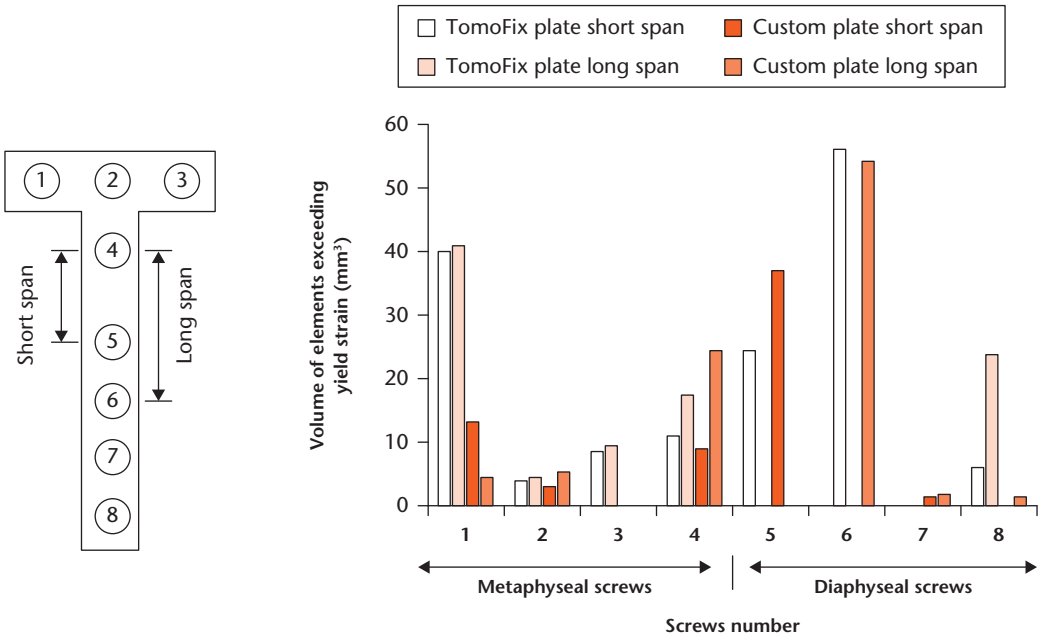

Fig. 9

Predicted volume of elements exceeding the yield strain of cortical bone (εVOL) for the different plates and screw configurations examined in the study. Results shown are for complete osteotomy gap (no callus healing).

specified optimization goal, the resulting plate stress could be substantially lower; however, the stiffness would be increased. To ensure the final plate design was flexible, we also included plate deformation as an equally weighted optimization goal.

Our study confirmed the findings of previous studies that increasing the bridging span increased the axial and transverse IFM.[38,39] Augat et al[40] demonstrated that transverse motion in the absence of axial motion can delay or prevent fracture healing. Park et al[41] showed that oblique motion (a combination of axial and transverse motion) produced the best healing in terms of callus formation. It is also known that intramedullary nails perform very well despite producing larger transverse movements than axial movements at the fracture site.[42] Therefore, provided that the device adequately stabilizes the fracture, the combination of transverse and axial IFM may be superior to predominantly or exclusively axial motion.

In previous studies that looked at locking plates, bridging span had a more pronounced influence on IFM than found in our study,[38,39] and we attributed this difference to two factors: 1) the orientation of the HTO plate with respect to the loading axis; and 2) the presence of the intact cortical hinge laterally. From the deformation observed in our models, it was clear that the plate bending was mainly around its major axis (the stiffer

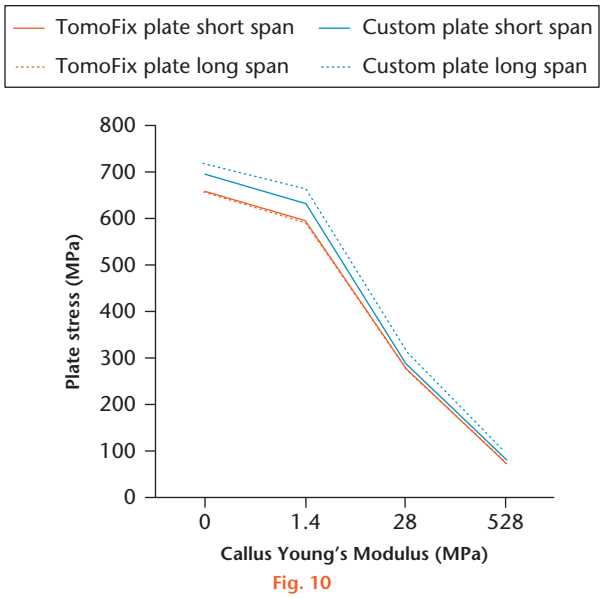

Fig. 10

Predicted von Mises stress in the different plate types and configurations for different levels of callus formation.

direction). Additionally, the intact lateral hinge resisted plate bending in the weak axis direction. It is likely that a complete osteotomy or a broken lateral hinge would substantially increase IFM.

The study predicted peak plate stresses in both plate designs to be lower than the yield strength of Ti-6Al-4V (approximately 789 MPa to 1013 MPa[43]). In our gap defect models, the plate stresses were much higher than the fatigue strength of titanium (approximately 150 MPa for fatigue fretting in phosphate-buffered saline[43]), indicating that callus healing is required to prevent fatigue failure.

Strain levels around screws can be indicative of loosening risk.[44,45] When using the TomoFix plate, our study predicted the strains within the bone to be largest in the proximal tibial fragment. This is the location where screw loosening and breakage have been reported to occur clinically,[46] giving us confidence in the clinical relevance of the modelling predictions. The optimized custom plate reduced strain levels in the proximal tibia where the bone stock is weaker. We attributed this finding to the increased amount of material surrounding the screws compared with the TomoFix plate – higher rigidity screws are known to reduce strain at the screw-bone interface.[47] One previous study reported a 6.7% rate of tibial plateau fracture; we did not investigate this aspect in our models, however, as the authors attributed it to a technical error of leaving too much lateral cortex intact.[48]

Martinez de Albornoz et al[49] conducted biomechanical experiments to evaluate IFM using different plate types and found larger values than the present study. Their study used low density synthetic bone and measured IFM at the loading actuator, making their results difficult to interpret. Other authors have measured much smaller displacements.[50,51] However, they used a highly constrained experimental setup, which is likely to have influenced the results.[31] Additionally, Röderer et al[51] measured very small values of IFM in one cadaveric model (0.05 mm at 1000 N) examining an alternative screw type, which they found dramatically increased the IFM to 0.16 mm at 1000 N. A previous experimental and computational study by Luo et al[28] used a similar loading regime to the present study and found IFM values for a TomoFix implant placed in the same orientation as the present study to be 0.93 mm at 2000 N.

This study has several important limitations. The operative technique for TomoFix includes the use of a compression screw to pull the plate closer to the bone, thus generating tensile preload in the plate and compressive preload in the lateral cortical hinge. We did not incorporate this phenomenon as it would be highly variable depending on the size of the hinge and the position of the plate. It would, however, alter predictions of plate stress, IFM, and εVOL. Validation was only conducted using the custom plate, and we assumed that the screw-plate contact parameters would be the same for the TomoFix plate. The experimental tests were primarily for validation purposes, with Sawbones selected for their consistent material properties.[25,52] Nevertheless, we only used a single specimen. It is difficult to compare our results with those of previous studies due to differences in loading regimes and geometrical variation such as the size of the lateral hinge, specimen dimensions, methods of restraining the specimens, and material properties. The material properties of third-generation Sawbones are different in compression and tension.[52] We chose to use the compressive Young's moduli as our test was a compression test, and implementing differing compressive and tensile moduli in FE codes is not straightforward. Moreover, the material properties of surrogate cortical bone may not be representative of human bone, particularly in osteoporotic cases. We considered the joint contact and muscle forces at 19% of the gait cycle. We also examined the influence of using forces corresponding to 44% of the gait cycle (second contact force peak) but found that it was not as critical for plate stress predictions. In our models, we evaluated the different plate types and configurations using predefined callus properties to represent different healing stages. It is known, however, that plates with larger IFM promote faster callus formation and thus also reduce plate stress more quickly.[53]

In conclusion, we found that larger bridging spans, particularly transverse movements, have the potential to increase substantially the IFM produced at the fracture site. Our optimized plate design produced similar plate stress to the TomoFix plate for both short and long bridging spans while substantially reducing high strain regions

within the bone. This study has shown that both plate types and spans produced very large plate stresses in the gap defect model. Substantial callus formation was required in all cases to reduce stress below the fatigue strength of titanium.

References

1. **Murphy L, Schwartz TA, Helmick CG, et al.** Lifetime risk of symptomatic knee osteoarthritis. *Arthritis Rheum* 2008;59:1207-1213.
2. **Nguyen USDT, Zhang Y, Zhu Y, et al.** Increasing prevalence of knee pain and symptomatic knee osteoarthritis: survey and cohort data. *Ann Intern Med* 2011;155:725-732.
3. **Patel A, Pavlou G, Mújica-Mota RE, Toms AD.** The epidemiology of revision total knee and hip arthroplasty in England and Wales: a comparative analysis with projections for the United States. a study using the National Joint Registry dataset. *Bone Joint J* 2015;97-B:1076–1081.
4. **Ruiz D Jr, Koenig L, Dall TM, et al.** The direct and indirect costs to society of treatment for end-stage knee osteoarthritis. *J Bone Joint Surg [Am]* 2013;95-A:1473–1480.
5. **Akizuki S, Shibakawa A, Takizawa T, Yamazaki I, Horiuchi H.** The long-term outcome of high tibial osteotomy: a ten- to 20-year follow-up. *J Bone Joint Surg [Br]* 2008;90-B:592–596.
6. **Kim MK, Ha JK, Lee DW, et al.** No correction angle loss with stable plates in open-wedge high tibial osteotomy. *Knee Surg Sports Traumatol Arthrosc* 2015;23:1999-2006.
7. **Pornrattanamaneewong C, Harnroongroj T, Chareancholvanich K.** Loss of correction after medial opening wedge high tibial osteotomy: a comparison of locking plates without bone grafts and non-locking compression plates with bone grafts. *J Med Assoc Thai* 2012;95(Suppl 9):S21-S28.
8. **Bonasia DE, Dettoni F, Sito G, et al.** Medial opening wedge high tibial osteotomy for medial compartment overload/arthritis in the varus knee: prognostic factors. *Am J Sports Med* 2014;42:690-698.
9. **Hankemeier S, Mommsen P, Krettek C, et al.** Accuracy of high tibial osteotomy: comparison between open- and closed-wedge technique. *Knee Surg Sports Traumatol Arthrosc* 2010;18:1328-1333.
10. **Wu L, Lin J, Jin Z, Cai X, Gao W.** Comparison of clinical and radiological outcomes between opening-wedge and closing-wedge high tibial osteotomy: A comprehensive meta-analysis. *PLoS One* 2017;12:e0171700.
11. **Woodacre T, Ricketts M, Evans JT, et al.** Complications associated with opening wedge high tibial osteotomy — A review of the literature and of 15 years of experience. *Knee* 2016;23:276-282.
12. **Warden SJ, Morris HG, Crossley KM, Brukner PD, Bennell KL.** Delayed- and non-union following opening wedge high tibial osteotomy: surgeons' results from 182 completed cases. *Knee Surg Sports Traumatol Arthrosc* 2005;13:34–37.
13. **Miller BS, Downie B, McDonough EB, Wojtys EM.** Complications after medial opening wedge high tibial osteotomy. *Arthroscopy* 2009;25:639–646.
14. **de Mello Junior WA, Arruda LR, Coluccini AM, et al.** Complications following medial opening wedge osteotomy of the knee: retrospective study. *Rev Bras Ortop* 2015;46:64–68.
15. **Spahn G.** Complications in high tibial (medial opening wedge) osteotomy. *Arch Orthop Trauma Surg* 2004;124:649–653.
16. **Simpson AHRW.** The forgotten phase of fracture healing: the need to predict nonunion. *Bone Joint Res* 2017;6:610–611.
17. **Nelissen EM, van Langelaan EJ, Nelissen RGHH.** Stability of medial opening wedge high tibial osteotomy: a failure analysis. *Int Orthop* 2010;34:217–223.
18. **MacLeod AR, Pankaj P.** Pre-operative planning for fracture fixation using locking plates: device configuration and other considerations. *Injury* 2018;49(Suppl 1):S12-18.
19. **Elliott DS, Newman KJH, Forward DP, et al.** A unified theory of bone healing and nonunion: BHN theory. *Bone Joint J* 2016;98-B:884–891.
20. **Diffo Kaze A, Maas S, Waldmann D, et al.** Biomechanical properties of five different currently used implants for open-wedge high tibial osteotomy. *J Exp Orthop* 2015;2:14.
21. **Jung WH, Chun CW, Lee JH, et al.** Comparative study of medial opening-wedge high tibial osteotomy using 2 different implants. *Arthroscopy* 2013;29:1063-1071.
22. **Schmidt U, Penzkofer R, Bachmaier S, Augat P.** Implant material and design alter construct stiffness in distal femur locking plate fixation: a pilot study. *Clin Orthop Relat Res* 2013;471:2808–2814.
23. **Hoffmeier KL, Hofmann GO, Mückley T.** Choosing a proper working length can improve the lifespan of locked plates. A biomechanical study. *Clin Biomech* 2011;26:405–409.
24. **Lujan TJ, Henderson CE, Madey SM, et al.** Locked plating of distal femur fractures leads to inconsistent and asymmetric callus formation. *J Orthop Trauma* 2010;24:156–162.
25. **Cristofolini L, Schileo E, Juszczyk M, et al.** Mechanical testing of bones: the positive synergy of finite-element models and in vitro experiments. *Philos Trans A Math Phys Eng Sci* 2010;368:2725–2763.
26. **Erdemir A, Guess TM, Halloran J, Tadepalli SC, Morrison TM.** Considerations for reporting finite element analysis studies in biomechanics. *J Biomechanics* 2012;45:625–633.
27. **Izaham RMAR, Kadir MRA, Muslim DA-J.** Screws placement effect on locking compression plate (LCP) for tibial oblique fracture fixation [abstract]. *Conference on Biomedical Engineering & Sciences (IECBES)*, Kuala Lumpur, Malaysia, 2010.
28. **Luo CA, Hwa SY, Lin SC, Chen CM, Tseng CS.** Placement-induced effects on high tibial osteotomized construct - biomechanical tests and finite-element analyses. *BMC Musculoskelet Disord* 2015;16:235.
29. **Pauchard Y, Ivanov TG, McErlain DD, et al.** Assessing the local mechanical environment in medial opening wedge high tibial osteotomy using finite element analysis. *J Biomech Eng* 2015;137:031005.
30. **Golovakha ML, Orljanski W, Benedetto K-P, et al.** Comparison of theoretical fixation stability of three devices employed in medial opening wedge high tibial osteotomy: a finite element analysis. *BMC Musculoskelet Disord* 2014;15:230.
31. **MacLeod A, Simpson AHRW, Pankaj P.** Experimental and numerical investigation into the influence of loading conditions in biomechanical testing of locking plate fracture fixation devices. *Bone Joint Res* 2018;7:111–120.
32. **MacLeod AR, Pankaj P, Simpson AHRW.** Does screw-bone interface modelling matter in finite element analyses? *J Biomech* 2012;45:1712–1716.
33. **Damm NB, Morlock MM, Bishop NE.** Friction coefficient and effective interference at the implant-bone interface. *J Biomech* 2015;48:3517-3521.
34. **Serrancolí G, Kinney AL, Fregly BJ, Font-Llagunes JM.** Neuromusculoskeletal model calibration significantly affects predicted knee contact forces for walking. *J Biomech Eng* 2016;138:81001.
35. **Isaksson H, Wilson W, van Donkelaar CC, Huiskes R, Ito K.** Comparison of biophysical stimuli for mechano-regulation of tissue differentiation during fracture healing. *J Biomech* 2006;39:1507–1516.
36. **Steiner M, Claes L, Ignatius A, et al.** Prediction of fracture healing under axial loading, shear loading and bending is possible using distortional and dilatational strains as determining mechanical stimuli. *J R Soc Interface* 2013;10:20130389.
37. **Ebacher V, Tang C, McKay H, et al.** Strain redistribution and cracking behavior of human bone during bending. *Bone* 2007;40:1265–1275.
38. **Stoffel K, Dieter U, Stachowiak G, Gächter A, Kuster MS.** Biomechanical testing of the LCP - how can stability in locked internal fixators be controlled? *Injury* 2003;34(Suppl 2):B11–B19.
39. **MacLeod AR, Simpson AH, Pankaj P.** Age-related optimization of screw placement for reduced loosening risk in locked plating. *J Orthop Res* 2016;34:1856–1864.
40. **Augat P, Burger J, Schorlemmer S, et al.** Shear movement at the fracture site delays healing in a diaphyseal fracture model. *J Orthop Res* 2003;21:1011–1017.
41. **Park SH, O'Connor K, McKellop H, Sarmiento A.** The influence of active shear or compressive motion on fracture-healing. *J Bone Joint Surg [Am]* 1998;80-A:868–878.
42. **Duda GN, Mandruzzato F, Heller M, et al.** Mechanical boundary conditions of fracture healing: borderline indications in the treatment of unreamed tibial nailing. *J Biomech* 2001;34:639–650.
43. **Hosseini S.** Fatigue of Ti-6Al-4V. In: Hudak R, Penhaker M, Majernik J, eds. *Biomedical Engineering - Technical Applications in Medicine*. Rijeka, Croatia: InTech, 2012:75-92.
44. **Giannoudis PV, Schneider E.** Principles of fixation of osteoporotic fractures. *J Bone Joint Surg [Br]* 2006;88-B:1272–1278.
45. **Turner CH, Anne V, Pidaparti RM.** A uniform strain criterion for trabecular bone adaptation: do continuum-level strain gradients drive adaptation? *J Biomech* 1997;30:555–563.
46. **Ming TS, Koon WM.** Autologous bone grafting and revision plating in a case of persistent high tibial osteotomy non-union. *J Orthop Case Rep* 2016;6:91-93.
47. **Donaldson FE, Pankaj P, Simpson AHRW.** Bone properties affect loosening of half-pin external fixators at the pin-bone interface. *Injury* 2012;43:1764–1770.
48. **Song EK, Seon JK, Park SJ, Jeong MS.** The complications of high tibial osteotomy: closing- versus opening-wedge methods. *J Bone Joint Surg [Br]* 2010;92-B:1245-1252.
49. **Martinez de Albornoz P, Leyes M, Forriol F, Del Buono A, Maffulli N.** Opening wedge high tibial osteotomy: plate position and biomechanics of the medial tibial plateau. *Knee Surg Sports Traumatol Arthrosc* 2014;22:2641–2647.

50. **Han SB, Bae JH, Lee SJ, et al.** Biomechanical properties of a new anatomical locking metal block plate for opening wedge high tibial osteotomy: uniplane osteotomy. *Knee Surg Relat Res* 2014;26:155–161.
51. **Röderer G, Gebhard F, Duerselen L, Ignatius A, Claes L.** Delayed bone healing following high tibial osteotomy related to increased implant stiffness in locked plating. *Injury* 2014;45:1648-1652.
52. **MacLeod AR, Rose H, Gill HS.** A validated open-source multi-solver fourth-generation composite femur model. *J Biomech Eng* 2016;138:124501.
53. **Comiskey DP, MacDonald BJ, McCartney WT, Synnott K, O'Byrne J.** The role of interfragmentary strain on the rate of bone healing-a new interpretation and mathematical model. *J Biomech* 2010;43:2830–2834.

Funding Statement

- We gratefully acknowledge the support of Arthritis Research UK (grant number: POC055) and Innovate UK (grant number: 102930). We also thank colleagues from the University of Bath including Stephen Coombes for help with instrumentation, Clare Ball for micro-CT scanning and Nick Waywell for experimental support.

Conflict of Interest Statement

- None declared